Ultra-Wideband Optical Modulation Spectrometer (OMS) Development

Grant NAG5-10476

Summary of Research

For the period 1 March 2001 through 29 February 2004

Principal Investigator:

Dr. Volker Tolls

July 2004

Prepared for
National Aeronautics and Space Administration Headquarters

Smithsonian Institution
Astrophysical Observatory
Cambridge, Massachusetts 02138-1596

The Smithsonian Astrophysical Observatory
is a member of the
Harvard-Smithsonian Center for Astrophysics

The Technical Officer for this Grant is Dr. Jonathan Gardner, Code SZ, National Aeronautics and Space Administration, Headquarters, Washington, DC 20546-0001

Optical Modulation Spectrometer

Introduction

The optical modulation spectrometer (OMS) is a novel, highly efficient, low mass backend for heterodyne receiver systems. Current and future heterodyne receiver systems operating at frequencies up to a few THz require broadband spectrometer backends to achieve spectral resolutions of R~10^5 to 10^6 to carry out many important astronomical investigations. Among these are observations of broad emission and absorption lines from extra-galactic objects at high redshifts, spectral line surveys, and observations of planetary atmospheres. Many of these lines are pressure or velocity broadened with either large half-widths or line wings extending over several GHz.

Current backend systems can cover the needed bandwidth only by combining the output of several spectrometers, each with typically up to 1 GHz bandwidth, or by combining several frequency-shifted spectra taken with a single spectrometer. An ultra-wideband optical modulation spectrometer with 10 - 40 GHz bandwidth will enable broadband observations without the limitations and disadvantages of hybrid spectrometers. Spectrometers like the OMS will be important for both ground-based observatories and future space missions like the Single Aperture Far-Infrared Telescope (SAFIR) which might carry IR/submm array heterodyne receiver systems requiring a spectrometer for each array pixel. Small size, low mass and small power consumption are extremely important for space missions.

This report summarizes the specifications developed for the OMS and lists already identified commercial parts. The report starts with a review of the principle of operation (Section 1), then describes the most important components and their specifications which were derived from theory (Section 2), and finishes with a conclusion and outlook (Section 3).

1. Principles of Operation

The operational principle of an Optical Modulation Spectrometer is quite simple [Tolls 2002]. Laser light with frequency f_0 is modulated by the intermediate frequency (IF) signal (with frequency range Δf) of a heterodyne receiver in an optical modulator (see Figure 1). The laser light leaving the modulator has acquired all frequencies $f_0 \pm m\Delta f$ (m is an integer) with amplitudes described by Bessel functions. This laser light illuminates a Fabry-Perot etalon. If a monochromatic laser with a divergent beam illuminates an etalon, the diffraction pattern created in the etalon by multiple beam interference would show the typical Fabry-Perot fringes, concentric dark and bright circles (Figure 1, left panel) [Born 1989]. For the OMS, the illuminating laser beam is sent through a cylindrical lens and is divergent only horizontally and parallel vertically. This illumination pattern creates a diffraction pattern consisting of bright and dark vertical lines (Figure 1, mid-left panel). All

these lines correspond to the same laser frequency, but for different multiples $m2\pi$ (interference order m) of the phase (Figure 1, phase plot to the mid-right). If the laser is modulated, we would get laser light with the frequencies f_0 and $f_0 \pm m\Delta f$. Thus, we would see the line signal as before accompanied by the two modulation sidebands at $f_0 \pm m\Delta f$ depicted by the grey areas in Figure 1 for the interference order m = 1. The response for the other interference orders would look similar. The right panel in Figure 1 shows the result of the demonstration of the OMS principle using an etalon with a finesse of only 100. It shows the lower sideband of the left fringe (order m=2) and the upper sideband for the right fringe (m=1) and a 6 GHz frequency synthesizer signal (marked with arrows) as seen by a 320 by 240 pixel InGaAs IR camera. For the OMS, only a single sideband is used and projected onto a linear detector array. The output signal of each detector is proportional to the intensity in its small frequency interval. As can be seen in Figure 1, the free spectral range (FSR) of the etalon needs to be at least twice the desired bandwidth of the spectrometer since the modulation of the laser always results in an upper and a lower sideband. In future this might change when suitable single sideband modulators become commercially available (currently they are under development, [Frankel 1998 and Loayssa 2003]).

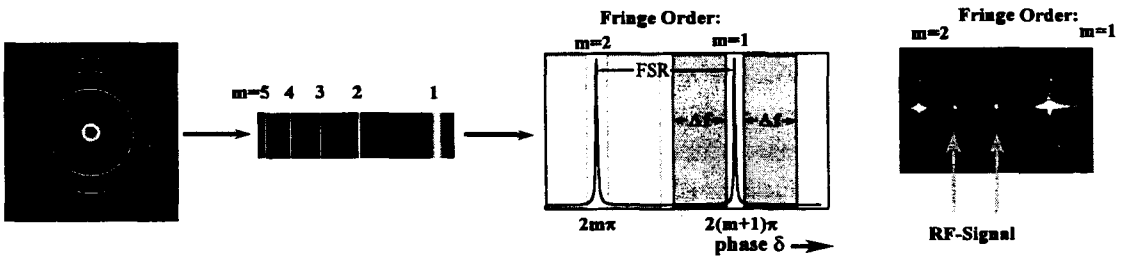

Figure 1: Schematic Fabry-Perot interference pattern for a divergent beam (left) and for a horizontally divergent and vertically parallel beam (center left). When the beam is horizontally divergent and vertically parallel, the frequency is dispersed over many orders in the horizontal direction (center). In the proposed OMS (center right), only a fraction of a single order (e.g., m = 7), denoted by the gray region with $f_0 + \Delta f$, is projected onto a linear CCD array. The OMS principle is demonstrated on the right showing the Fabry-Perot fringes as seen by an IR array camera (R. Schieder, University of Cologne). The two marked RF-signals are the response of the test setup to a 6 GHz synthesizer signal. The left spot belongs to the lower sideband of the left fringe and the right spot to the upper sideband of the right fringe. The etalon had a finesse of 100.

A schematic of the optical design is shown in Figure 2. The light from the laser diode module is fed into the modulator using an optical fiber cable. In the modulator, the laser light is modulated by the RF signal coming from the heterodyne receiver. The modulated output signal is formed after another fiber cable and a fiber-to-free-space transition into a parallel light beam. A cylindrical lens matches the horizontal divergence of the laser beam to the OMS specific angular acceptance range of the etalon. The output light of the etalon is imaged onto a detector array.

2. Optical Components

The main components of the OMS are the electro-optical modulator, the laser diode with

fiber optic interface, the Fabry-Perot etalon, and the linear detector array. In the following paragraphs, the essential specifications for these components will be derived and discussed. The discussion is mainly applicable to specific requirements for an OMS.

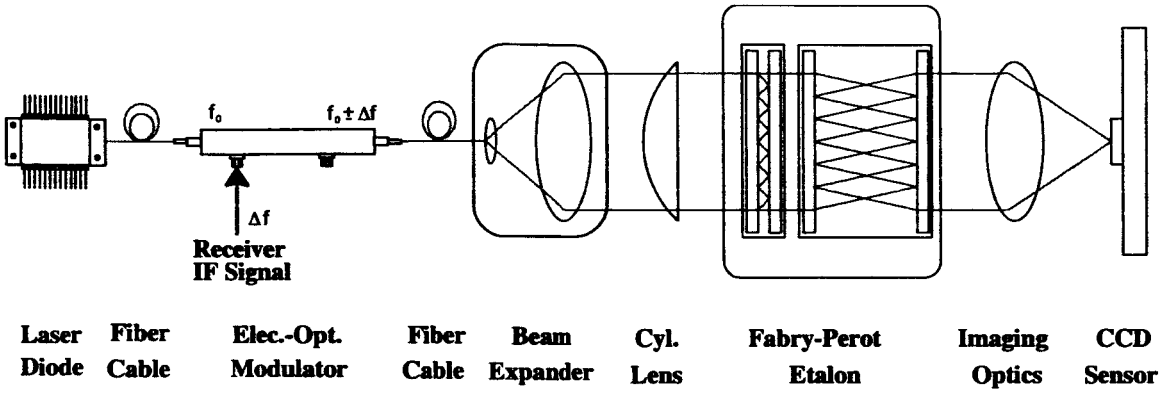

Figure 2: Schematic of an OMS.

2.1 Modulator

The most common types of broadband modulators are electro-optical modulators, based on the electro-optical effect in material like $LiNbO_3$, and electro-absorption modulators, based on the electro-absorption effect in material like InP. Other types of modulators include traveling wave modulators, polymer modulators, Pockels cells, etc. Currently, the best choice for an OMS is the external electro-optical modulator. The configuration of electro-optical modulators is shown in Figure 3 for a phase modulator (left panel) and for an intensity modulator (right panel). The phase modulator shows the simple, basic design. An optical waveguide in a $LiNbO_3$ crystal is covered by an electrode which is surrounded by grounding planes. If a modulation signal is applied to the electrode, the light traveling through the waveguide is phase modulated. The main disadvantage of the phase modulator is that only a small fraction of the laser light is modulated, and both the modulated laser light and the unmodulated laser carrier are passed through.

The drawing of the intensity modulator in Figure 3 shows a single input Mach-Zehnder configuration (multiple input Mach-Zehnder modulators are of no interest for the OMS). In this configuration, the incoming light is split in equal parts in a Y-junction into two waveguides. If no RF-signal is applied to the electrodes, the two signals are recombined at the second Y-junction and coupled into a single output. Since the two signals have the same phase, their amplitudes add to the almost full input signal. If a RF-voltage is applied to the electrodes, the refractive index in the $LiNbO_3$ material changes due to the electro-optical effect and the signal in one waveguide is advanced and in the other one retarded. When both signals are recombined in the Y-junction, they no longer add up but cancel

out (if the phase difference is 180 degrees which can be adjusted by means of a bias voltage).

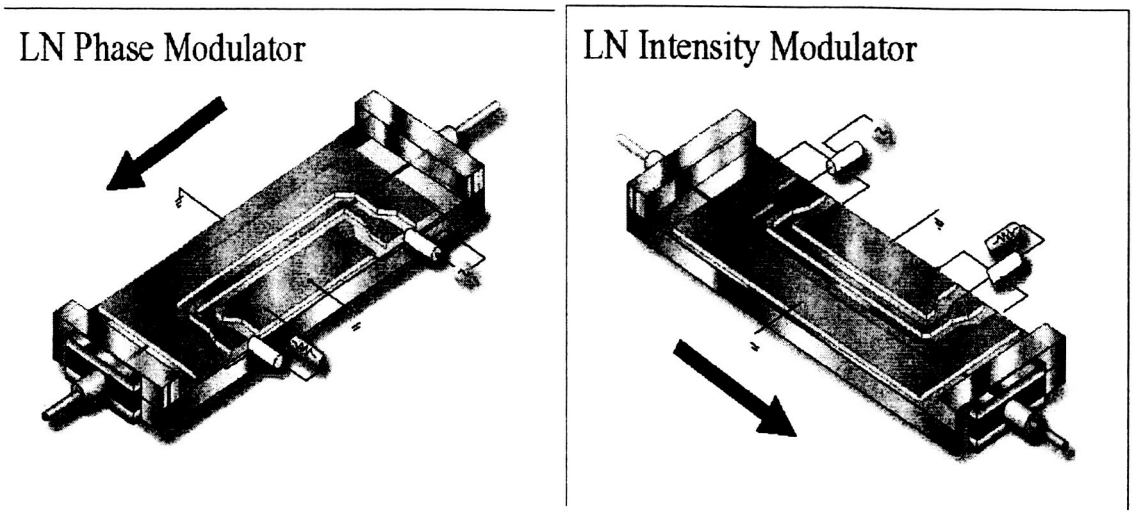

Figure 3: Common types of broadband modulator configurations: Phase modulator (left) and Intensity modulator (right). (Figures from Sumitomo 2002)

The transfer function of a Mach-Zehnder modulator can be written as (see, e.g., [Li 2003]):

$$I = I_0 \cos^2\left(\frac{\pi V}{2V_\pi} - \frac{\Phi}{2}\right)$$

with: V_π: voltage required to achieve π optical phase shift
V: input voltage (RF signal)
I_0: optical input power
I: modulated optical output power
Φ: static bias phase shift

It is common practice to set the static bias phase shift to the Quadrature Bias Point: $\Phi = \pi/2$. At this point, the input signals are transformed into optical signals by switching voltage to both sides of the Quadrature Bias Point (see Figure 4). Applying this and setting $\cos^2(\alpha) = 0.5(\cos 2\alpha + 1)$ leads to:

$$I = \frac{I_0}{2}\left[1 + \cos\left(\frac{\pi V}{V_\pi} - \Phi\right)\right] = \frac{I_0}{2} + \frac{I_0}{2}\sin\left(\frac{\pi V}{V_\pi}\right) \approx \frac{I_0}{2} + \frac{I_0 \pi V}{2V_\pi} - \frac{I_0 \pi^3 V^3}{8V_\pi^3}$$

An alternate approach would be to assume that the input voltage is sinusoidal and consists of two or more frequency components. Then, the cos-part of the last equation can be

expanded into a series of Bessel functions. This needs to be done to calculate the 3rd order intermodulation product for large input voltages (for a detailed analysis, see, e.g., [Kolner 1987]). For the input voltage ranges we are interested in, the previous approximation is sufficient.

The first term in the las equation defines the operating point, the second term is the linear modulation dependence, and the third term describes the 3rd order intermodulation product. However, either the resulting amplitudes are linearized by the calibration software, or the modulator can be operated at RF power levels such that the 3rd order intermodulation product is negligibly small (η_{NL} is the permitted non-linearity):

$$I_{3rd} / I_0 = \frac{\pi^3}{8}\left(\frac{V}{V_\pi}\right)^3 = 3.9\left(\frac{V}{V_\pi}\right)^3$$

$$I_{3rd} / I_0 \le \eta_{NL}\frac{\pi V}{2V_\pi} \Rightarrow V / V_\pi \le \sqrt{\eta_{NL}\frac{4}{\pi}}$$

An input voltage of less than 0.11 V_π is required to keep the 3rd order modulation below η_{NL}=1% and of less than 0.16 V_π for η_{NL}=2%.

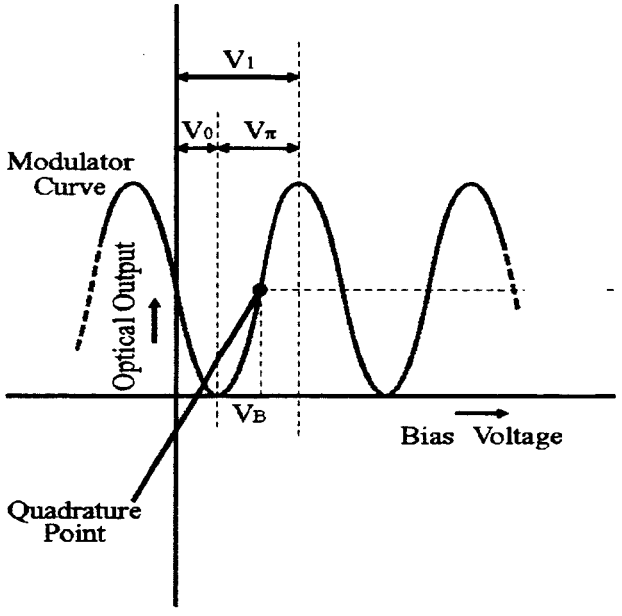

Figure 4: Quadrature Bias Point

Among the various types of modulators, we consider the best choice a Mach-Zehnder modulator. The advantage of this modulator compared to a standard phase modulator, as it was used by the University of Cologne (UC) for demonstrating the OMS principle, is the much higher suppression of the 0th-order laser light. Figure 5 shows the initial results from the UC demonstration. The spectrum shows a large effect of the unmodulated laser light, its line wing, and sidelobes. Even with suppressing the 0th-order laser light in an external interferometer by about 15 dB, the remaining 0th-order laser light amplitude is

still larger than the signal amplitude. In a Mach-Zehnder modulator, the interferometer is integrated into the modulator and can be adjusted using the bias signal to the modulator. An experiment conducted by Covega Corporation [Covega 2003], a promising supplier of a 40 GHz bandwidth, shows the high suppression of the 0^{th}-order laser light in their modulator. Figure 6, grey/purple curve, shows the 0^{th}-order laser light in an unbiased modulator with no RF signal applied and the modulated laser light (black/dark blue curve). The 0^{th}-order laser light amplitude is successfully suppressed by more than 25 dB. The additional 10 dB suppression over the UC experiment would reduce the carrier signal in Figure 5, right panel, by an additional factor of 10 or to <25000 counts. The remaining signal would just be detectable and, therefore, it should have no effect on the remaining spectrum.

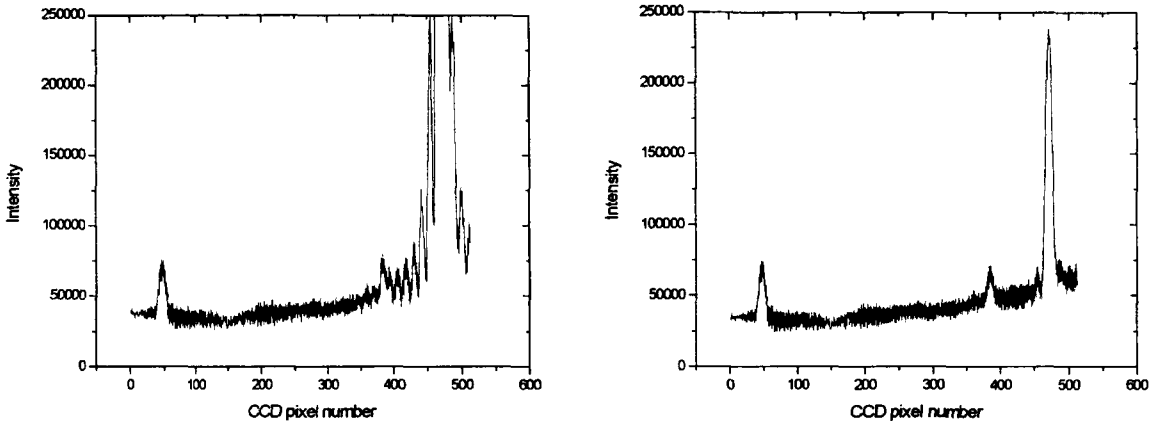

Figure 5: Result of University of Cologne demonstration of the OMS principle. The left plot shows the results without external interferometer and the right side with external interferometer to suppress the laser light carrier.

The efficiency of the modulator can be derived from the Covega measurement which gives an amplitude of the modulate light of >-7dB relative to the amplitude of the un-modulated light. The non-linearity criterion above shows that we should only use a modulator drive voltage of 0.11 V_π (approximately -10 dB). Thus, the laser light amplitude is attenuated by about -17dB.

Besides the mentioned Covega modulator, suitable modulators are available from manufacturers such as Agere Technologies [Agere 2002] and JDS Uniphase [2002]. Both companies offer 40 GHz bandwidth modulators in various configurations.

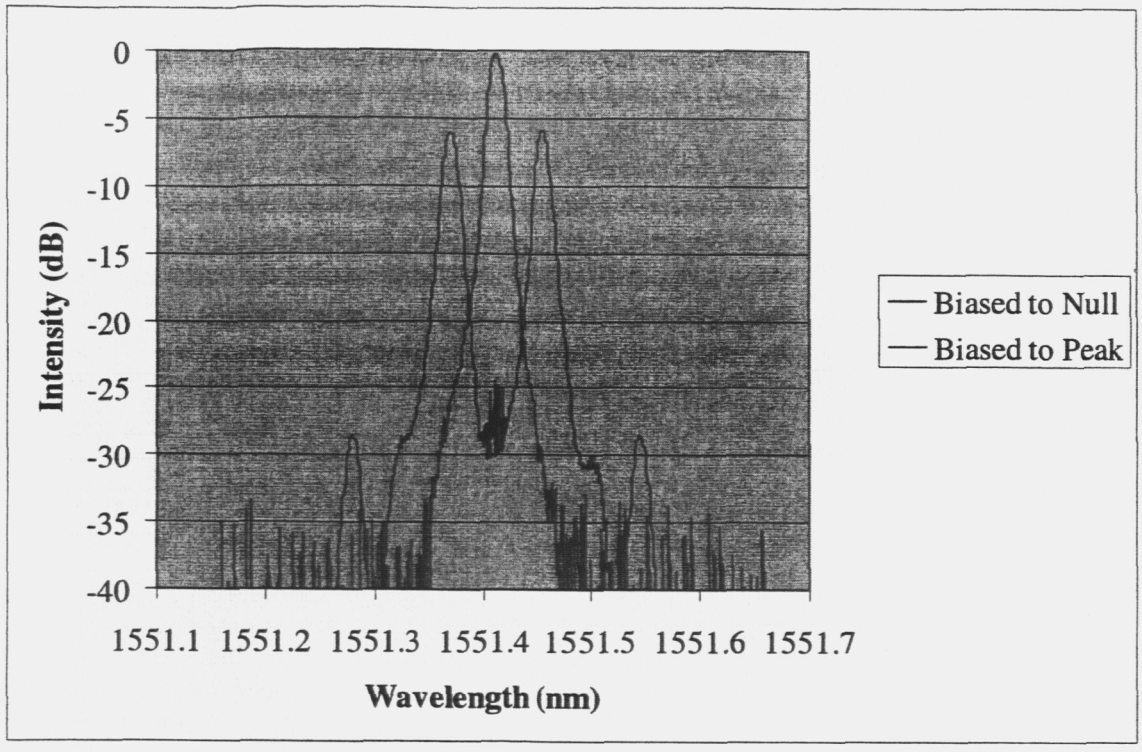

Figure 6: Transmission of a broadband Covega modulator [Covega 2003]. The purple curve shows the unmodulated carrier transmission of the modulator. The blue curve shows the modulated light with a suppression of >25 dB of the unmodulated light (the drive voltage was V_π).

2.2 Diode Laser

During the boom in the telecommunication industry, much research was done to improve the characteristics of laser diodes at 1550 nm. Many of these laser diodes operate in a single longitudinal mode with typical linewidths of $\Delta\lambda < 1$ MHz ([Agere 2001] and JDS Uniphase CQF 935/708 Series [JDS 2002]) fulfilling the OMS laser diode requirement of $\Delta\lambda < 5$ MHz (1/2 pixel FWHM is the minimum linewidth, and <1/10 pixel FWHM is optimal). The other requirement set for the OMS is the wavelength stability of $\partial\lambda/\partial T < 2$ MHz/minute. The absolute wavelength is not very important as long as it is about 1550 nm. This stability requirement can be achieved by temperature stabilizing the laser diode, and/or by locking the laser onto the Fabry-Perot etalon with electrical feedback to the laser diode current or temperature control circuitry; these methods are well established in laser spectroscopy. A review of several methods can be found in [Wieman 1991] and referenced papers therein. The temperature stabilization is made easier because almost all laser diodes for telecommunications have integrated thermo-electric coolers.

Programmatically, for the development of the OMS, 10-20 laser diodes should be purchased and tested for their individual performance. The best performing laser diode

should be used for the OMS development while the remaining will be kept as spares. This method proved to be successful for the selection of the laser diodes used in the Submillimeter Wave Astronomy Satellite (SWAS) AOS ([Klumb 1995] since the manufacturer's tolerances are less stringent than the OMS requirements and the performance varies greatly even within a single production run. Thus, suitable laser diodes are readily available.

2.3 Detector

At the laser wavelength of 1550 nm, the only available line detector array with 1024 pixels is manufactured by Sensors Unlimited, Inc. The SU1024LE array [SU 2001] is a linear InGaAs focal plane array (FPA) sensitive to radiation from 800 nm to 1700 nm. The pixel size is 25 x 500 μm with a 25 μm pitch. The most important parameters are listed in Table 2.1.

Table 2.1: Sensors Unlimited, Inc., SU1024LE linear detector array performance characteristics. The application in an OMS requires operating the detector in the high dynamic range. Values for the high sensitivity mode can be taken from the data sheet.

Wavelength range	0.8 – 1.7	μm	
Responsivity	10.5	nV/photon	
Quantum Efficiency	>70	%	
Gain	15.4	nV/electron	*1
Readout noise	10,000	electrons/√(scan)	*1,*2
Dark rate	1.9 1.23×10^8	V/s e^-/s	*1
Full-well capacity	1.3×10^8	electrons	*1
Pixel size	25x500	μm	
# pixels	1024		

*1: high dynamic range mode
*2: the read noise depends nearly linearly on temperature (as it is primarily k_bTC/q noise)

2.3.1 Detector Noise Sources

The important sources of noise in a focal plane array are: photon shot noise, dark current shot noise, Johnson noise, flicker noise, and read noise from the focal plane array readout circuitry. See discussion in Sensors Unlimited's application note "The Sensitivity of Focal Plane Arrays and Cameras."

a) For InGaAs, 1/f or flicker noise is negligible for frequencies of more than 1 Hz. At the light levels expected for the OMS application, it can be completely neglected.

b) Shot noise: $\left\langle I_S^2 \right\rangle^{1/2} = \sqrt{2qBI_{dark}}$

q	Charge of electron, $1.602\ 10^{-19}$ C
B	Measurement bandwidth, $B = 1/(2\,t_{int})$
t_{int}	integration time
I_{dark}	Dark current

The integrated noise charges are:

$$Q_S = \left\langle I_S^2 \right\rangle^{1/2} t_{int} = \sqrt{2qBI_{dark}}\, t_{int} = \sqrt{\frac{2qI_{dark}}{2t_{int}}}\, t_{int} = \sqrt{qt_{int} I_{dark}}$$
$$= \sqrt{qQ_{dark}} = \sqrt{qNq} = q\sqrt{N}$$

And the number of shot noise electrons is:
$N_S = \sqrt{N_{dark}}$

c) Johnson noise: $\left\langle I_J^2 \right\rangle^{1/2} = \sqrt{\frac{4k_B TB}{R}}$

k_B	Boltzmann's constant, $1.380\ 10^{-23}$ J/K
T	Temperature, K
R	Photodiode impedance

For the SU1024LE linear detector array we get:

$$\left\langle I_J^2 \right\rangle^{1/2} = \sqrt{\frac{4\,1.380\cdot 10^{-23}\ 0.5}{3\cdot 10^9}}\sqrt{t_{int}} = 9.59\cdot 10^{-17}\sqrt{t_{int}}$$
$$Q_J = \left\langle I_J^2 \right\rangle^{1/2} t_{int} = 9.59\cdot 10^{-17} t_{int}^{3/2}$$
$$N_J = \frac{Q_J}{q} = \frac{9.59\cdot 10^{-17}}{1.602\cdot 10^{-19}} t_{int}^{3/2} = 600\, t_{int}^{3/2}$$

The total noise is (not including the signal shot noise):

$$N_{tot} = \sqrt{\left(N_S^2 + N_J^2 + N_R^2\right)} = \sqrt{\left(N_{dark} + 3.6 \cdot 10^5\, t_{int}^3 + 10^8\right)}$$
$$= \sqrt{\left(1.23 \cdot 10^8\, t_{int} + 3.6 \cdot 10^5\, t_{int}^3 + 10^8\right)}$$

Assuming an integration time t_{int} = 10ms, the dominant noise source is the read noise. At about 1 s integration time, the read noise would equal the shot noise, but the detector would be inoperable since the dark electrons alone would fill the well. Thus, the final integration time is determined by the signal level on the detector and the number of dark electrons allowed. For an integration time of 10 ms, the number of dark electrons is less than 1/100 of the full well capacity resulting in a dynamic range of >20 dB. It needs to be determined to what extend cooling would increase the dynamic range.

2.4 Etalon

A Fabry-Perot etalon (FPE) consists of 2 highly reflective plane parallel mirrors illuminated near normal incidence. The most important parameters are the free spectral range (FSR) and the finesse (for details regarding Fabry-Perot etalons see, e.g. [Born 1989]). The FSR is the frequency difference of light that produces identical interference rings (compare Figure 3) and is determined by the separation of the mirrors. The required FSR for an OMS with 10 GHz bandwidth is >20 GHz. In order to allow for sufficient separation between the upper and lower modulation sidebands of adjacent fringe orders (compare Figure 3), the FSR should be > 22 GHz. For a 40 GHz OMS, the FSR should be > 88 GHz. The finesse specifies the frequency resolution of the FPE. For an OMS with 10 GHz bandwidth and 10 MHz resolution, the finesse should be larger than the ratio FSR/resolution; for example, for the 10 GHz OMS we get: finesse > 22 GHz/10MHz = 2200 (such an FPE would have an optical resolving power of $2 \cdot 10^7$ at 1550 nm).

2.4.1 Free Spectral Range

The **free spectral range (FSR)** $\delta\upsilon$ is defined as (e.g. [Born & Wolf 1989]):

$$\delta\upsilon = \frac{c}{\Delta s} = \frac{c}{2d\sqrt{n^2 - \sin^2(\theta)}}$$

and for $\theta = 0$:

$$\delta\upsilon = \frac{c}{2nd} \quad \text{or} \quad d = \frac{c}{2n\delta\upsilon}$$

with:

Δs path length difference,

d etalon thickness,
n refractive index of etalon material,
θ angle of incidence.

For a 40-GHz bandwidth OMS, the FSR must be larger than twice the bandwidth to have no overlap between the upper and lower sidebands of adjacent orders. Including an additional margin of 10%, the required FSR is 88 GHz. For solid etalons at visible to near-IR wavelengths, the typical material is fused quartz with a refractive index of 1.444 at 1550 nm wavelength. Table 2.2 summarizes etalon thicknesses for OMS important bandwidths. Combination a would be required for a 40 GHz bandwidth OMS and Combination b for a 10 GHz bandwidth OMS.

Table 2.2: Specifications for the OMS etalons. Combination a would be for a 40 GHz bandwidth OMS and Combination b for a 10 GHz bandwidth OMS.

Bandwidth (GHz)	Thickness d (mm)	Remark
88	1.18	Combination a
22	4.73	Combination b
4	26.04	Combination a
1	104.17	Combination b

2.4.2 Finesse

The **reflective finesse** F_R (often only referred to as finesse) of an etalon is only a function of the reflectivity of the etalon mirrors (assuming both mirrors have the same reflectivity as usually is the case), e.g. [Born & Wolf 1989]:

$$F_R = \frac{\pi\sqrt{R}}{1-R}$$

For low finesse etalons, the reflectivity is the determining factor. If the finesse approaches 100 or higher finesse is required, the surface accuracy cannot be neglected when calculating the total finesse. For a surface with an surface accuracy of λ/x (typically $\lambda/20$ to $\lambda/100$), the surface finesse F_S is:

$$F_S \approx x$$

The surface accuracy includes the microscopic surface defect (e.g. roughness of surface) and the macroscopic, large-scale surface defects (e.g. slightly convex or concave surface and wedge effects between the plane-parallel surfaces).

They both combine to the total finesse F:

$$F = \sqrt{F_R^2 + F_S^2}$$

2.4.3 Transmitted Intensity

Since we are using etalons only in transmission, we will only look at the transmitted intensity. Similar equations regarding reflected intensity can be found in the literature.
The transmitted intensity I_t is described by the Airy function (e.g. [Born & Wolf 1989]):

$$I_t = I_0 \frac{1}{1 + F \sin^2(\delta/2)}$$

$$F = \frac{4R}{(1-R)^2}$$

$$\delta = 2\pi \Delta s / \lambda + \Delta\varphi$$

$$\Delta s = 2d \sqrt{n^2 - \sin^2(\theta)}$$

with:

I_0 incident intensity,
R reflectivity,
λ wavelength,
$\Delta\varphi$ path,
d etalon thickness,
n refractive index of etalon material,
θ angle of incidence.

In case there is absorption in the etalon mirror surfaces or the etalon material, we have:

$$I_t = I_0 \frac{T^2}{(A+T)^2} \frac{1}{1 + F \sin^2(\delta/2)}$$

In the presence of absorption, $A > 0$, the additional factor is always $\frac{T^2}{(A+T)^2} < 1$. For dielectrical mirrors, A is typically around 0.3% resulting in a loss of the transmitted intensity (assuming an R of 97%) of 19% (81% of the incident light is transmitted - these values do not include coupling losses which are about 3-4 dB).

2.4.4 Imaging Optics

The required parameters for the imaging optics are the focal length and the aperture. The aperture needs to be larger than the etalon diameter (see Section 2.4.4) in order to avoid aperture effects.

The focal length of the imaging optics depends on the desired resolution and bandwidth of the OMS. To derive an equation to calculate the focal length required to achieve the desired resolution on the detector, we first have to derive the diameters of the fringes, an etalon can produce when illuminated with monochromatic light. We are starting with:

$$m\lambda = 2nd\cos(\beta)$$

β is the angle of the light within the etalon. Now we are setting: $m = m_0 - p$ with the number of rings p starting with $p = 0$ for the central ring. Without limiting us, we assume that we have no fractional interference order and the central ring is degraded to a point:

$$m_0 = \frac{2nd}{\lambda} \quad for \quad \beta = 0,\ p = 0$$

$$(m_0 - p)\lambda = 2nd\cos(\beta_p) = 2nd(1 - \frac{\beta_p^2}{2}) = 2nd(1 - \frac{1}{2}\left(\frac{n_0}{n}\right)^2 \alpha_p^2) \quad for \quad \beta \ll 1,\ p > 0$$

Subtracting the two equations yields the (outside) angle α_p for the p^{th} ring:

$$\alpha_p^2 = \frac{\lambda np}{n_0^2 d}$$

The output beam of the etalon is imaged with a lens with focal length f, we derive for the diameter D_p and the radius r_p of the p^{th} ring:

$$D_p = 2r_p = 2f\alpha_p = \sqrt{\frac{4np\lambda}{n_0^2 d}} f \text{ or}$$

$$f = \sqrt{\frac{n_0^2 d}{np\lambda}} r_p$$

In the OMS we want to operate in the lowest possible order of the etalon: $p = 1$. In order to size the focal length properly, we remember that the FSR needs to be twice the design-bandwidth of the OMS to separate the upper from the lower sideband. Then, our linear

detector array (number of pixels n_{pix} = 1024 pixel, pixel width w_{pix} = 25 μm) should cover this range which is about half of the radius of the first ring. Since we are using a solid etalon, the refractive index $n_0 = 1$, and n is the refractive index of the etalon material (e.g., fused silica: n = 1.444 @ 1550 nm):

$$f = \sqrt{\frac{d}{n\lambda}}\, 2n_{pix}\, w_{pix}$$

In case of a double etalon, d is the thickness of the etalon that determines the bandwidth of the OMS. For the 40 GHz bandwidth OMS (d = 1.12 mm, see Table 2.1) we get a focal length of:

$$f = \sqrt{\frac{0.0012m}{1.444*1.55\cdot 10^{-6}m}}\, 2*1024*25\cdot 10^{-6}m = 1.2m$$

The required focal length is quite large. Further investigation should focus on the design of optics incorporating the large focal length into small volumes by means of folded optics.

2.4.5 Size of Etalon

The thickness of the etalon was covered in an earlier paragraph. Now the question is the diameter of the etalon. There are two effects to be considered when sizing the etalon: 1) diffraction effects should be smaller than spectral features and 2) there must be a sufficient number of reflections within the etalon to achieve the desired spectral resolution.

Effect 1): when considering diffraction from the aperture of the etalon with diameter D, we have to fulfill the requirement for the angular resolution:

$$\partial\upsilon \approx 1.22\frac{\lambda}{D}$$

which should be smaller or equal to the angular resolution defined by the finesse of the etalon:

$$d\upsilon = \sqrt{\frac{FSR}{2\theta\lambda c}}\,\frac{\lambda}{F}$$

The wavelength λ constrains the thickness of the etalon to $2d = p\lambda$ with p an integer. F is the finesse of the etalon. Setting $\partial\upsilon \leq d\upsilon$, we can calculate the required diameter of the etalon (Schieder 2001):

$$D \geq \sqrt{\frac{2\theta\lambda c}{FSR}}\, F$$

For a wavelength $\lambda = 1550\, nm$, $\alpha = 1$, a free spectral range $FSR = 88\, GHz$, and a finesse $F = 200$ we get:

$$D \geq 2.1\, cm$$

Effect 2): Vaughan defines the following two numbers for his treatment of finite etalon apertures:

$$k \approx \frac{D}{d\theta} \quad \text{and} \quad n \approx \frac{A-D}{2d\theta}$$

with an entrance diameter D, an exit diameter A, an etalon thickness d, and an entrance angle θ. Since we are going to use etalons with A=D, the second parameter is always 0. He states that effects of the finite aperture are negligible for $k \geq 200$. For $k \approx 100$, the line width, contrast, and peak intensity are degraded by 10 - 20 %. For $k \approx 40$ these parameters are degraded by a factor of 2. The corresponding values for the 40 GHz bandwidth OMS are k≈700 for the thinner etalon and k≈150 assuming an etalon diameter of 25 mm. Thus, the available etalon diameter should have no negative effect on the performance.

2.4.6 Double Etalons

Initially, a single Fabry-Perot etalon was considered for the OMS. However, early into the study it became clear that this etalon would require a clear aperture of >250mm. Such an aperture combined with the separation of the etalon surfaces and their accuracy is technically not feasible (at least not for the development of an OMS). Therefore, the design was changed to incorporate the proven method of utilizing a two-etalon system with a clear aperture of >25mm (see, e.g. [Hernandez 1986], [Vaughan 1989]). The first etalon has low resolution and the desired FSR; for the OMS we suggest a finesse of 25 and a FSR of 22 GHz (88 GHz for the 40 GHz bandwidth version). The second etalon has high resolution and a smaller FSR which must be an integer fraction of the first etalon's FSR. For the OMS we suggest a finesse of 100 and a FSR of 1 GHz (5 GHz respectively for the 40 GHz bandwidth version). Both etalons in series act like a single etalon with a finesse of 2500 and a FSR of 22 GHz (88 GHz respectively). The only difference is that the double etalon has spurious spectral features at known locations (produced by the second etalon with the smaller FSR) with amplitudes of 10^{-3} to 10^{-4} of the strongest signal in the band. These can easily be removed by software if required. Both etalons will be solid etalons which are readily available as modified off-the-shelf components from vendors like VLOC, CVI Laser, or Optics for Research (OFR).

2.4.7 Thermal Considerations

It is well known that etalons are very sensitive to thermal changes. Therefore it is an important matter for the OMS to get an initial guess of its thermal sensitivity.

If the optical path length in the etalon changes by $\lambda/2$ then the fringes have moved by one FSR. Therefore, we can only allow a path length change which moves the fringe only by 1/3 of a pixel or $1.7 \cdot 10^{-4}$ FSR (assuming 2000 pixel per FSR) or the optical path length in the etalon can change by $8.3 \cdot 10^{-5} \lambda$:

$$\Delta d = d(T_0)\, \alpha\, \Delta T = 8.3 \cdot 10^{-5}\, \lambda \quad \Rightarrow \quad \Delta T = \frac{8.3 \cdot 10^{-5}\, \lambda}{d(T_0)\, \alpha}$$

The path length change will be more severe in the larger etalon. For the 40 GHz OMS we get:

$$\Delta T = \frac{8.3 \cdot 10^{-5}\, \lambda}{d(T_0)\, \alpha} = \frac{8.3 \cdot 10^{-5}\, 1.55 \cdot 10^{-6}}{0.026\ \ 0.5 \cdot 10^{-6}} = 9.9 mK$$

A thermal stability of 9.9 mK should be easily possible through thermal stabilization of the etalons. However, the design of the OMS should still incorporate a feedback loop between the thermal stabilization of the thicker etalon (the thermal effects are about 25 times more severe as for the smaller etalon) and the location of the remaining carrier signal on the detector. If this location can be held steady, thermal effects in the etalon are compensated for and should not affect the performance of the spectrometer.

2.5 OMS Throughput

The following Table 2.3 shows how much light will hit the detector. The modulator efficiency has been estimated from the Covega measurements.

Table 2.3: Throughput of OMS and estimated electron counts in detector.

Optical Interface	Gain/Loss	Unit	Remark
Laser Diode w/pig tail	10	dBm	10 mW laser diode
Coupling to Modulator	-4	dB	
Modulation Efficiency	-17	dB	all frequency elements
Coupling to Fiber	-4	dB	value might be reduced by immediate transition to free space
Transition to Free Space	-2	dB	
Loss @ Cylindrical Lens	-1	dB	
Coupling to Etalon	-2	dB	
Transmitted Intensity Etalon 1	-3	dB	50% transmission estimated
Transmitted Intensity Etalon 2	-3	dB	50% transmission estimated
Loss @ Imaging Optics	-1	dB	
Coupling to Detector	-1	dB	Beam slightly out of focus to reduce sensitivity
Intensity on Detector (per pixel)	-28	dBm	
	1.58E-06	Watt	
Photons on Detector	1.24E+13	ph/sec	
Photons per frame	2.47E+11	ph	20 ms integration time
Measured electrons	1.98E+11	e-	quantum efficiency: 80%
Electrons per pixel	1.98E+08	e-	1000 pixels
Relative well capacity	1.52		1.3 10^8 e- well capacity

Remark: The unmodulated light is suppressed by >25dB in the modulator. This means that its intensity is by about 8dB lower than the single-line intensity of the modulated line. Therefore, the unmodulated light is still measurable on the CCD detector, but it is no longer a major source for stray light. Fortunately, it can even be used to compensate for remaining thermal drifts. Its position can be measured with high accuracy and an error signal can be derived to change the set-point of the laser diode temperature control (changing the temperature of the laser diode slightly changes its wavelength accordingly) to compensate for any position changes. Whether such a stabilization is required must be determined with an engineering model OMS (the thermal dependence did not really require one).

3 Conclusion and Outlook

The goal of this study was to lay the groundwork for successful development of an Optical Modulation Spectrometer. In the previous section it was shown that an OMS can be built with commercially available components with customized development in a few areas. The most important area will be the thermal stabilization of the OMS. However, the means for a straightforward stabilization are given. The derivation of an error signal is easy for the OMS. It is actually fortunate that the laser carrier signal can be measured on the detector without compromising the spectroscopic measurements. Its signal strength can be adjusted within limits by means of the bias signal required for the modulator operation. Then, the carrier signal on the detector can be analyzed (like a comb sig-

nal for frequency calibration) in the data processing computer which in return will generate a bias signal for the temperature stabilization. The remaining tasks will be to adjust the stabilization parameters (e.g., the time constants for the stabilization circuitry). All other areas are well understood.

The study presented suggests solid etalons. However, further investigation may reveal whether air-space etalons might improve the performance since they can be built with higher resolution. Whether air-space etalons improve the spectral performance of the OMS can only be tested in an engineering model and not a more theoretical study.

Another area where continued industrial advances might lead to improvements is the development of single sideband modulators (see, e.g.[Frankel 1998] and [Loayssa 2003]). Single sideband modulators would lead to a reduction of the required FSR easing the constraints on etalons even more.

The last area that might profit from industrial developments is the detector. In future, detector arrays with more than 1024 pixels might be developed increasing either the covered bandwidth or the spectral resolution without sacrificing bandwidth.

Since the groundwork is done and the principle has been demonstrated, the next step is to build an engineering model for real performance testing.

Partial results of this study have been published in:
Tolls, V., and Schieder, R., "Optical Modulation Spectrometer: A Concept Study," in Proc. Of "Thirteens International Symposium on Space Terahertz Technology," Cambridge, MA, USA, March 26-28, 2002

4 References

Agere Systems, Data Sheet "Wavelength-Selected D2525P Isolated DFB Laser Module with PMF," July 2001

Agere Systems, Data Sheet "40 GBits/s Lithium Niobate Electro-Optical Modulator," January 2002

Born, M. and Wolf, E "Principles of Optics," Pergamon Press, Oxford 1989

Covega Corp., priv. communication, 2003

Covega Corp., Data Sheet "Mach-40™ 40 Gb/s Intensity Modulator," 2004

Davis, C.C., "Laser and Electro-Optics," Cambridge University Press, Cambridge, 2000

Demtroeder, W., "Laser Spectroscopy," Springer Series in Chemical Physics 5, Springer, Berlin, 1982

Frankel, M.Y., and Esman, R.D., J. Lightwave Tech., Vol. 16, 5, 859-863, 1998

Hernandez, G. "Fabry-Perot Interferometers," Cambridge University Press, Cambridge, 1986

JDS Uniphase, Data Sheet, "40 mW 1550 nm CW DFB Laser with PM Fiber for WDM Applications," Rev. 02, Jan. 2002

Klumb, M., et al., "Acousto-Optical Spectrometers for spaceborne applications," Proc. SPIE, Vol. 2583, 420, 1995

Kolner, B.H., and Dolfi, D.W., Appl. Optics, Vol. 26, 17, 3676-3680, 1987

Li, G.L., and Yu, P.K.L., J. Lightwave Tech., Vol. 21, 9, 2010-2030, 2003

Loayssa, A., Lim, C., Nirmalathas, A., and Benito, D., J. Lightwave Tech, Vol. 21, 4, 1071-1081, 2003

Schieder, R. priv. comm., 2001

Schieder, R. "Back-End Spectrometers," Post-Herschel Workshop, Madrid, 2003

Sensors Unlimited, Inc., Data Sheet, "SU1024LE-1.7 InGaAs Linear Photodiode Array," 2003

Sensors Unlimited, Inc., Application Note, "The Sensitivity of Focal Plane Arrays and Cameras," Rev.B, Doc. No. 4110-0029, 2004

Sumitomo, "Application Note for LN modulator," July 2002

Tolls, V., and Schieder, R., "Optical Modulation Spectrometer: A Concept Study," in Proc. Of "Thirteens International Symposium on Space Terahertz Technology," Cambridge, MA, USA, March 26-28, 2002

Wieman, C.E., and Hollberg, L. Rev. Sci. Instrum. **62**, 1, 1991

Vaughan, "The Fabry-Perot Interferometer," Adam Hilger, Bristol, 1989